# Controller for Fast Frequency Response from Variable Frequency Induction Motor Drives with Centrifugal Torque Loads


Zarka Mirza
*Department of Hydro and Renewable Energy*
*Indian Institute of Technology (IIT) Roorkee*
Uttarakhand, India
zarka_m@hre.iitr.ac.in

Himanshu Jain
*Department of Hydro and Renewable Energy*
*Indian Institute of Technology (IIT) Roorkee*
Uttarakhand, India
himanshu.jain@hre.iitr.ac.in



***Abstract*—With the increasing integration of inverter-based renewable energy sources such as solar PV and wind, modern power systems are facing inertia-related challenges. This paper presents a demand-side solution to address this issue by proposing a grid-supportive controller for variable-frequency induction motor drive operating with a centrifugal torque load under field-oriented control (FOC). The controller was validated in software through MATLAB/Simulink simulations, which showed that for a 2.5% frequency change during an over- and under-frequency event and a 5% droop coefficient, the drive was able to increase and decrease its power by around 50% within 0.1 seconds, respectively. Reducing the droop setting to 3%, increased the power modulation to approximately 83%. The results demonstrate that these loads can provide accurate and predictable droop control and effectively provide Fast Frequency Response (FFR) and support grid frequency stability.**



***Index Terms*—Grid Supportive Load, Field-Oriented Control, droop control, centrifugal loads, synthetic inertia, grid-integration, climate change, and demand flexibility.**


## I. Introduction

The increasing share of inverter-based variable renewable energy (VRE) sources, such as solar photovoltaic (PV) and wind power, has led to a decline in grid inertia, as these systems lack the rotating masses found in conventional generators [1]. Although synthetic inertia can be introduced in them through advanced control methods, doing so typically requires reserving power headroom, which can result in renewable curtailment and reduced energy utilization [2]. As renewable penetration continues to grow, managing the resulting inertia deficit will become increasingly challenging. Grid-supportive technologies such as small hydropower plants, battery energy storage systems, pumped storage plants, flywheels, supercapacitors, grid-forming inverters, and synchronous condensers are potential solutions to mitigate these issues [1]. Along with these solutions, demand response (DR) has also emerged as a promising complementary solution for addressing inertia-related challenges in inverter-dominated power systems [1], [3]–[6].

Unlike traditional load-shifting programs, modern DR enables fast, automated power modulation based on local measurements, allowing loads to participate in real-time grid balancing [3], [4]. Autonomous Demand Response (ADR) projects like the Grid Friendly Appliance (GFA) initiative have shown that household appliances can react to grid frequency changes within a fraction of a second [5], while the Olympic Peninsula Project confirmed the feasibility of automated HVAC control under dynamic pricing conditions [7]. These studies have demonstrated that DR-enabled loads can respond to frequency deviations within short timeframes and contribute to frequency regulation [5]–[7].

Reference [8] introduced the concept of Grid-Supportive Loads (GSLs), which are large inverter-based loads such as HVAC systems, Electric Vehicle chargers, variable-frequency drives (VFDs), and refrigeration units that have the potential to provide grid support but currently lack such embedded functionality. It was shown that integrating 20% of GSLs into an ERCOT 2k-bus system improves the frequency response by 2000 MW/0.1 Hz and reduces the frequency nadir deviation by nearly 60%.

Recent studies have further demonstrated that inverter-based loads can contribute to frequency regulation by adjusting their power consumption in response to local frequency measurements [9]–[13]. Large populations of variable-speed drives have been experimentally shown to provide droop-like primary frequency response [9], while induction motor drives and household appliances have exhibited autonomous frequency-support capability without communication or adverse impact on operation [10], [11]. Furthermore, experimental studies have shown that embedding grid-supportive control in VFDs supplying constant-torque loads can deliver fast frequency response (FFR) within sub-second time scales [12].

While prior studies have demonstrated the feasibility of frequency-responsive VFDs, existing approaches largely focus on constant-torque loads or aggregated system-level behaviour. Limited attention has been given to device-level control design for VFDs with centrifugal torque loads, such that these loads accurately modulate their power in accordance with the droop law.

To address these gaps, this paper presents: (i) a grid-supportive control functionality for VFDs supplying centrifu-

979-8-3315-8138-1

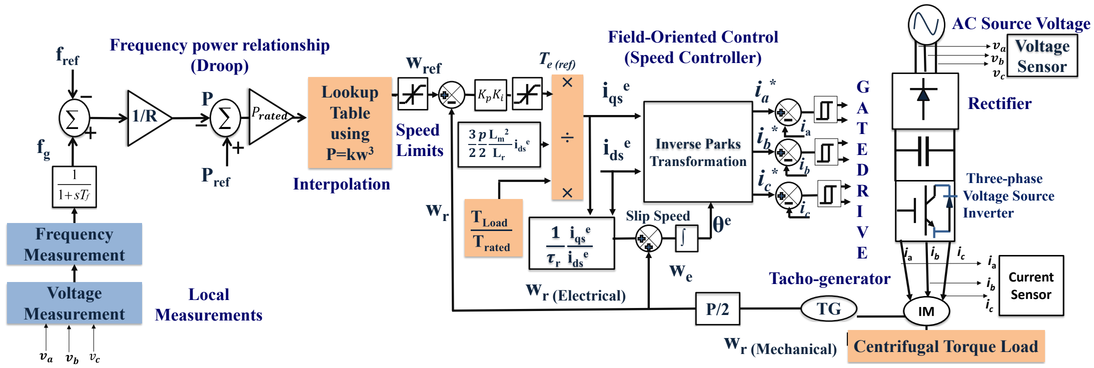


Fig. 1: Grid-supportive functionality added to the variable-frequency induction motor drive with centrifugal load.

gal torque loads, together with a modified field-oriented control (FOC) speed controller, enabling accurate under- and over-frequency support across multiple droop coefficients while strictly adhering to the droop law and providing predictable, controlled power modulation; and (ii) a significant improvement in response time, reducing from 1 s to 0.1 s.

The remainder of this paper is organised as follows. Section II describes the grid-supportive control algorithm for centrifugal torque loads. Section III presents and discusses the simulation results, and Section IV concludes the paper with remarks on future work.

## II. Grid-supportive Control Algorithm for Variable Frequency Induction motor Drives with Centrifugal Torque Loads

Centrifugal loads are suitable for implementing grid-supportive functionalities, as they consume a considerable share of electrical power. Examples of large-scale centrifugal loads are water pumping stations, HVAC systems, boiler feed pumps, and industrial compressors [14]. These loads are governed by affine laws, where torque ($T$) varies with the square of motor speed ($\omega_r$) and power consumption of the load ($P$) varies with the cube of speed. This section introduces a grid-supportive controller designed for centrifugal torque loads to enable automatic power modulation and provide FFR. The proposed controller allows these loads to automatically modulate their power consumption in response to frequency changes based on a droop control to provide a controlled and predictable response, thereby delivering both under- and over-frequency support within FFR timeframes while maintaining their inherent affine characteristics. The droop control for loads is implemented such that the percentage change in power ($\%\Delta P$) equals the ratio of the percentage change in grid frequency ($\%\Delta f_g$) to the droop coefficient ($\%R$). Mathematically, droop law formulation is shown in (1).

$$\%\Delta P = \frac{1}{\%R}\%\Delta f_g \tag{1}$$

Figure 1 shows the block diagram of the proposed controller integrated with a VFD operating a centrifugal torque load, and the controller architecture comprising the two main components is described next.

### A. Grid Supportive Functionality

The proposed controller can add grid-supportive functionality and modulate the power of the VFD driving the centrifugal load based on grid frequency ($f_g$) only if real-time frequency measurement is available. Instead of relying on external devices such as smart meters or phasor measurement units, a local frequency measurement approach can be employed. In this method, the grid voltage input to the VFD is scaled down using a potential divider circuit, and the reduced voltages ($v_a$, $v_b$, $v_c$) are fed to the controller, where techniques such as phase-locked loop (PLL) or zero-crossing detection are used to estimate the grid frequency locally. This measured grid frequency is fed to the droop control to adjust the VFD power output according to grid frequency changes and the selected droop coefficient. Under this control, the VFD decreases power when the frequency falls and increases power when it rises, by decreasing and increasing speed, respectively, thereby enabling FFR. This objective is achieved by generating a reference speed ($\omega_{ref}$) from the reference power command ($P_{ref}$), which is computed using droop-based modulation using ($f_g$), reference frequency ($f_{ref}$), ($\%R$), rated VFD power ($P_{rated}$), and reference power $P_{ref}$, as given in (2)–(5).

$$P - P_{ref} = \frac{f_g - f_{ref}}{\%R} \tag{2}$$

In per-unit form, the droop relationship becomes (3).

$$\frac{P - P_{ref}}{P_{ref}} = \frac{f_g - f_{ref}}{f_{ref}} * \frac{1}{\%R} \tag{3}$$

$$P(p.u) - 1 = \frac{f_g(p.u) - 1}{\%R} \tag{4}$$

The corresponding reference power is obtained as (5)

$$P_{ref} = P(p.u) * P_{rated} \tag{5}$$

For centrifugal torque loads, $\omega_{ref}$ corresponding to the $P_{ref}$ is generated using cubic interpolation based on the cubic power–speed characteristic of the load, given by (6)

$$\omega_{ref} = \left(\frac{P_{ref}}{k}\right)^{\frac{1}{3}}; \omega_{min} \leq \omega_{ref} \leq \omega_{max}; k = \frac{P_{rated}}{\omega_{rated}^3} \tag{6}$$

979-8-3315-8138-1

TABLE I: Validation of Droop Control for Centrifugal Load.

| Parameter | Case 1 | Case 2 | Case 3 | Case 4 |
|---|---|---|---|---|
| $f_g$ (Hz) | 58.50 | 58.50 | 61.50 | 61.50 |
| $R$ (%) | **5** | **3** | **5** | **3** |
| $\omega_{ref}$ (rad/s) | 118.90 | 82.49 | 172.81 | 187.72 |
| $\omega_r$ (rad/s) | 118.92 | 82.48 | 172.78 | 187.74 |
| $T_L$ (Nm) | 8.49 | 4.91 | 17.94 | 21.14 |
| $T_e$ (Nm) | 9.19 | 4.56 | 18.84 | 22.31 |
| $P$ (W) | 1010 | 338.4 | 3097.11 | 3968.16 |
| $\%\Delta f_g$ | **2.5** | **2.5** | **2.5** | **2.5** |
| $\%\Delta P$ (theoretical (1)) | **50.00** | **83.33** | **50.00** | **83.33** |
| $\%\Delta P$ (simulated) | **49.60** | **83.36** | **52.00** | **94.80** |

where $k$, $\omega_{rated}$, $\omega_{min}$, and $\omega_{max}$ are proportionality coefficient, rated speed, minimum speed limit, and maximum speed limit, respectively.

The generated $P_{ref}$ is mapped on the lookup table created using (6) to generate $\omega_{ref}$ for the speed controller of the VFD. When $\omega_{ref}$ reaches the predefined minimum or maximum limits, the motor saturates and no further power modulation occurs.

### B. Speed Controller

Modern smart appliances commonly employ three-phase motor drives using FOC which is a well-established speed controller, which enables independent control of the torque- and flux-producing components of the stator current [15]. This decoupled control allows smooth operation across the entire speed range and ensures high dynamic performance with rapid speed tracking capability.

To integrate grid-supportive functionality into VFDs driving centrifugal loads under FOC, modifications are introduced to ensure compliance with the controlled and predictable droop control. The quadrature current component $i_{qs^e}$ generated in the FOC algorithm is further scaled by the ratio of the load torque $T_{Load}$ to the rated torque $T_{rated}$ of the drive before being applied to the inverse Park's transformation and slip speed control as shown in (7) and Fig. 1.

$$i_{qs^e} = \frac{T_{e(ref)}}{\frac{3pL_m^2}{4L_r} i_{ds^e}} * \frac{T_{Load}}{T_{rated}} \tag{7}$$

where $T_{e(ref)}$, $p$, $L_m$, $L_r$, and $i_{ds^e}$ are reference electromagnetic torque, number of poles, mutual inductance, rotor inductance, and direct component of the current, respectively. The resulting slip speed $(\omega_e)$ obtained from the slip speed control is integrated to obtain the slip angle $(\theta^e)$, which is used in the inverse Park's transformation to generate the reference phase currents $(i_a^*, i_b^*, i_c^*)$. These reference currents are compared with the measured phase currents $(i_a, i_b, i_c)$ and processed by a hysteresis current controller to generate the inverter switching pulses.

Thus, the integration of local frequency measurement, droop-based power control, cubic interpolation for speed reference generation, and a modified FOC scheme enables controlled and predictable droop-law-compliant power modulation in VFDs supplying centrifugal torque loads.

## III. Results and Discussion

The proposed control algorithm was validated through MATLAB/Simulink simulations using the setup shown in Fig. 1, comprising the controller; a VFD of 4 poles, 60 Hz, 460 V, and 3730 W; and a centrifugal torque load $T_L$ of 13.5 Nm. The simulations were executed on a 12th Gen Intel(R) Core(TM) i7-12700 processor. The centrifugal torque load was modeled using a lookup table representing the quadratic speed-torque relationship. The values of $L_r$, $L_m$, rotor resistance $r_r$, $i_{ds}^e$, $i_{qs}^e$, proportional gain $(K_p)$, and integral gain $(K_i)$ were 0.0597 H, 0.0237 H, and 1.083 Ω, 1 A, 0.6 A, 13, and 26, respectively. The values of various parameters in the grid functionality part of the control algorithm, $P_{ref}$, $P_{rated}$, $f_{ref}$, $T_{rated}$, filter time constant $T_f$ were 1 pu., 3730 W, 22 Nm, 60 Hz, and 0.05 s, respectively. Under- and over-frequency events were simulated using step changes in frequency using a three-phase programmable voltage source (415 V, 60 Hz) which inherently had low impedance. The simulations assume an ideal grid voltage source with negligible source impedance and accurate local frequency measurement to isolate and evaluate the proposed control strategy. The VFD adjusted its power accordingly following the algorithm described in Section II.

Four simulation cases, as discussed below, were conducted to validate the controller performance and quantify the FFR capability of the VFD with centrifugal torque load.

- Case 1: Underfrequency Event with R=5%
- Case 2: Underfrequency Event with R=3%
- Case 3: Overfrequency Event with R=5%
- Case 4: Overfrequency Event with R=3%

The frequency deviations considered in this study fall within the abnormal operating and ride-through ranges specified in IEEE 1547-2018 for inverter-based resources, which define allowable under- and over-frequency limits around the nominal grid frequency [16].

Fig. 2 shows the response of the VFD with a centrifugal load during under- and overfrequency events for Simulations (1-4). Fig. 2a through 2f show parameters such as the grid frequency $f_g(n)$, reference rotor speed $\omega_{refn}$, rotor speed $\omega_{rn}$, load torque $T_{Ln}$, electromagnetic torque $T_{en}$, power $P_n$, and percentage deviation in power for a particular $\%R$ $\Delta P_n^{\%R}$ where $n$ is the case number.

For Simulations 1-4, the values of $\omega_{refn}$, $\omega_{rn}$, $T_{Ln}$, $T_{en}$, and $P_n$ at a grid frequency of 60 Hz are 150 rad/s, 149.995 rad/s, 13.5 Nm, 14.46 Nm, and 2024 W, respectively. At $t = 5\,\mathrm{s}$ after the under and overfrequency event, the grid frequencies $f_g$ change to 58.5 Hz and 61.5 Hz, respectively. Table I summarizes the parameters and percentage changes observed at the frequency nadir for the four cases. It also compares the simulated percentage changes in power with those estimated theoretically using (1). The major observations from Fig. 2 and Table I are discussed next.

### A. Underfrequency Response from Centrifugal Torque loads

Fig. 2 illustrates the under-frequency response obtained from the VFD with centrifugal torque load. As the grid

979-8-3315-8138-1

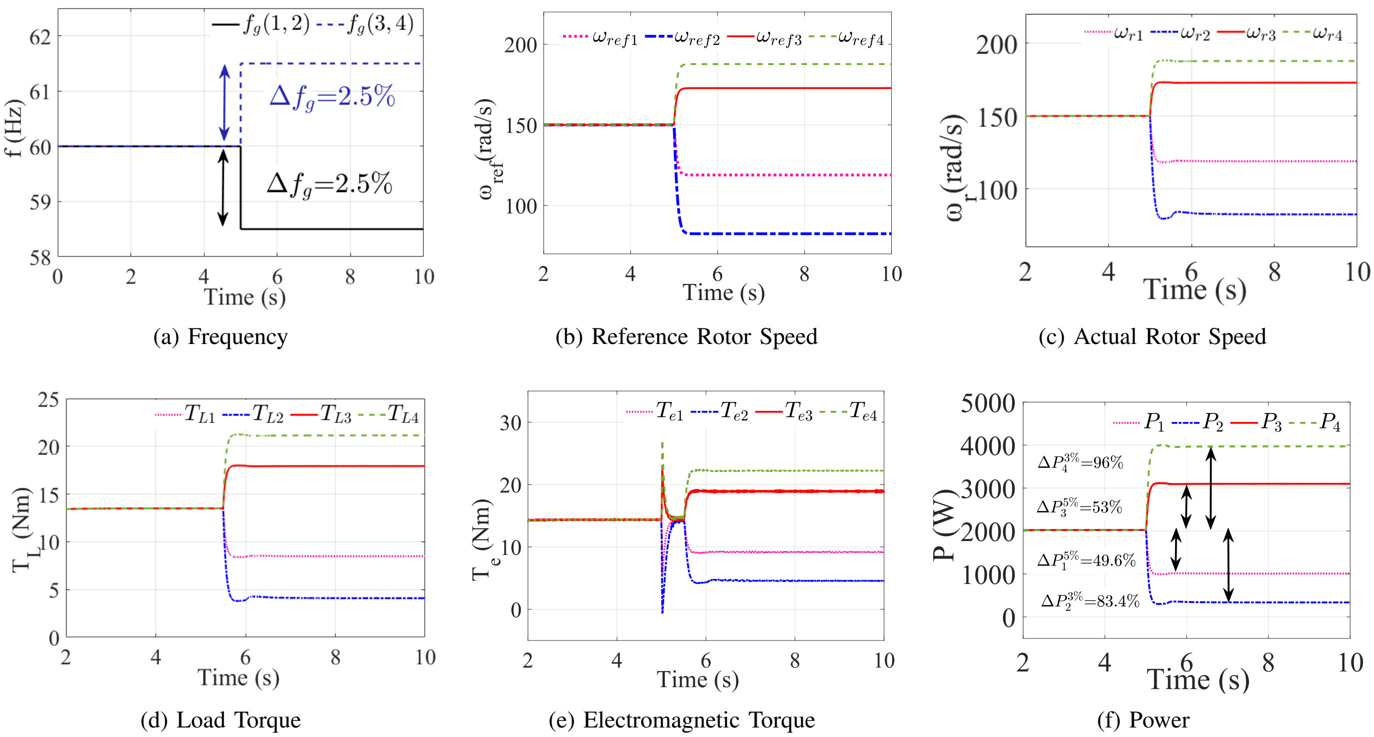


(a) Frequency (b) Reference Rotor Speed (c) Actual Rotor Speed

(d) Load Torque (e) Electromagnetic Torque (f) Power

Fig. 2: FFR for under-frequency (Case 1, and 2) and over-frequency events (Case 3 and 4) .

frequency decreases to 58.5 Hz at t=5 s, both rotor speed and power reduce accordingly. For the two under-frequency cases ( Case 1 and 2), the rotor speeds decreased to 118.92 rad/s and 82.48 rad/s, while the corresponding power outputs dropped to 1010 W and 338.4 W, respectively, thereby demonstrating the load's capability to provide under-frequency response by automatically reducing power within FFR timeframes.

### B. Overfrequency Response from Centrifugal Torque load

Fig. 2 illustrates the over-frequency response obtained from the VFD with centrifugal torque load. As the grid frequency increases to 61.5 Hz at t=5 s, both rotor speed and power rise accordingly. For the two over-frequency cases (Cases 3 and 4), the rotor speeds increased to 174 rad/s and 190 rad/s, while the corresponding power outputs rose to 3097.11 W and 3968.16 W, respectively, demonstrating the load's capability to provide over-frequency response by increasing power within FFR timeframes.

### C. Droop Control

As per the droop control in (1), a 2.5% change in frequency with 5% and 3% droop settings should result in 50% and 83.3% changes in power, respectively. For the under-frequency events (Cases 1 and 2) shown in Fig. 2 and Table I, the power decreased by 49.6% and 83.36% for 5% and 3% droop settings, respectively. Similarly, for the over-frequency events (Cases 3 and 4) shown in Fig. 2 and Table I, the power increased by 52% and 94.8% for 5% and 3% droop settings, respectively, confirming that the system response closely follows the controlled and predictable droop control.

### D. Affine Law for Centrifugal Torque Loads

In Case 1, when the grid frequency drops at $t = 5$ $s$, the speed decreases from 149.99 rad/s to 118.92 rad/s i.e., speed reduces by almost $\frac{4}{5}$ times its initial value. The load torque and power decrease proportionally by $(\frac{4}{5})^2$ and $(\frac{4}{5})^3$, as shown in Fig. 2 and Table III. In Case 4, at $t = 5$ $s$, the speed increases from 149.9 rad/s to 187.74 rad/s i.e., the speed increases by almost $\frac{5}{4}$ times its initial value, which leads to increases in torque and power by $(\frac{5}{4})^2$ and $(\frac{5}{4})^3$, respectively. These results show that the affine characteristics of centrifugal torque loads are maintained, indicating that the droop control embedded in the controller does not alter their inherent behavior. Table III presents the validation of affine relationships for all four cases.

### E. Response Time

The FFR time-frame is generally between 0-2 s. Fig. 2 show that when the frequency event occurs at t=5 s, the load responds within 0.1 s and modulates its speed and power with respect to the frequency, thus providing FFR.

### F. Comparison with the Previous Work

Fig. 3 and Table III compare the theoretical and simulated power modulation and response time of the proposed method with [13]. In [13], a 2.5% drop in grid frequency with a 5% droop setting results in an approximately 87% reduction in power for a centrifugal load, whereas droop control predicts a

979-8-3315-8138-1

TABLE II: Validation of Affine Law for Centrifugal Load.

| Ratio | Under-Frequency | | Over-Frequency | |
|---|---|---|---|---|
| | Case 1 | Case 2 | Case 3 | Case 4 |
| $\omega_r^{new}/\omega_r^{old}$ | $4/5$ | $11/20$ | $23/20$ | $5/4$ |
| $T^{new}/T^{old}$ | $(4/5)^2$ | $(11/20)^2$ | $(23/20)^2$ | $(5/4)^2$ |
| $P^{new}/P^{old}$ | $(4/5)^3$ | $(11/20)^3$ | $(23/20)^3$ | $(5/4)^3$ |

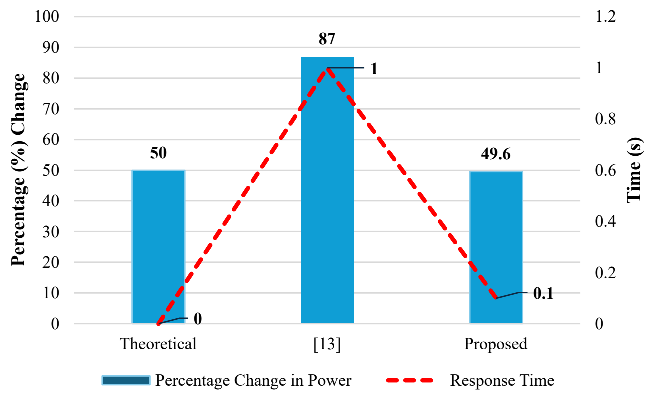


Fig. 3: Comparison of theoretical and simulated power change and response time for [13] and the proposed method.

50% reduction, yielding an overresponse with an absolute error of $+37\%$. This occurs because a control algorithm designed for constant-torque loads is directly applied to a centrifugal torque load.

The proposed method achieves a 49.6% power reduction for the same frequency deviation and droop coefficient (Case 1 in Fig. 2 and Table I), closely matching the droop-law prediction with an absolute error of only -0.4%. For a reduced droop coefficient of 3%, a 2.5% frequency deviation results in an 83% power reduction, as expected. Furthermore, the response time is improved from 1 s to 0.1 s. Unlike [13], the proposed controller also demonstrates over-frequency response capability. Hence, the modified control algorithm enables controlled and predictable droop-based power modulation for centrifugal torque loads with improved FFR.

## IV. Conclusion

This paper presents a grid-supportive controller to integrate controlled and predictable droop response functionality into induction motor drives operating with centrifugal torque loads under FOC speed control. Simulation results demonstrate that the proposed controller enables these drives to automatically provide both over- and under-frequency responses within FFR timeframes. For a 2.5% change in grid frequency with a 5% droop setting, the centrifugal torque load adjusted its power output by approximately 50% within 0.1 s while maintaining its inherent affine characteristics. When the droop setting was reduced to 3%, the power modulation increased to approximately 83%, confirming the controller's effectiveness.

In future work, the proposed controller will be evaluated on inverter-driven centrifugal torque loads, such as pumps and HVAC compressors, using hardware-in-the-loop or hardware

TABLE III: Comparison between [13] and proposed work.

| Metric | Under-Frequency | | Over-Frequency | |
|---|---|---|---|---|
| | [13] | Proposed | [13] | Proposed |
| $\%\Delta f$ | $-2.5\%$ | $-2.5\%$ | $-$ | $+2.5\%$ |
| $\%R$ | $5\%$ | $5\%$ | $-$ | $5\%$ |
| $\%\Delta P(theoretical)$ | $50\%$ | $50\%$ | $-$ | $50\%$ |
| $\%\Delta P(simulated)$ | $87\%$ | $49.6\%$ | $-$ | $53\%$ |
| Absolute Error | $+37\%$ | $-0.4\%$ | $-$ | $+3\%$ |
| Response Time | $1s$ | $0.1s$ | $-$ | $0.1s$ |

validation to demonstrate their grid-support capability. Furthermore, system-level studies will be conducted to assess the aggregated impact of grid-supportive VFDs on overall grid performance.

## References


[1] Z. Mirza, H. Jain, From challenges to solutions: Review and analysis of grid-supportive technologies in sustainable power systems, Applied Energy 403 (2026) 127111.

[2] S. Saha, M. Saleem, T. Roy, Impact of high penetration of renewable energy sources on grid frequency behaviour, International Journal of Electrical Power & Energy Systems 145 (2023) 108701.

[3] E. Tsybina, C. Winstead, B. Ollis, M. Olama, T. Kuruganti, Demand response for frequency regulation: Research continuity and knowledge gaps, Renewable and Sustainable Energy Reviews 207 (2025) 114958.

[4] R. Jurjevic, T. Zakula, Demand response in buildings: A comprehensive overview of current trends, approaches, and strategies, Buildings 13 (10) (2023) 2663.

[5] D. J. Hammerstrom, J. Brous, D. P. Chassin, G. R. Horst, R. Kajfasz, P. Michie, T. V. Oliver, T. A. Carlon, C. Eustis, O. M. Jarvegren, et al., Pacific northwest gridwise™ testbed demonstration projects; part ii. grid friendly™ appliance project, Tech. rep., Pacific Northwest National Lab.(PNNL), Richland, WA (United States) (2007).

[6] F. K. Tuffner, Electric vehicle standards–grid service capabilities: Evaluation of ieee 2030.13, sae j3072, iso 15118-2, iso 15118-20, ocpp, iec 61850-7-420, ieee 2030.5, and openadr, Tech. rep., Pacific Northwest National Laboratory (PNNL), Richland, WA (United States) (2024).

[7] D. J. Hammerstrom, R. Ambrosio, T. A. Carlon, J. G. DeSteese, G. R. Horst, R. Kajfasz, L. L. Kiesling, P. Michie, R. G. Pratt, M. Yao, et al., Pacific northwest gridwise™ testbed demonstration projects; part i. olympic peninsula project, Tech. rep., Pacific Northwest National Lab.(PNNL), Richland, WA (United States) (2008).

[8] H. Jain, B. Mather, A. K. Jain, S. F. Baldwin, Grid-supportive loads—a new approach to increasing renewable energy in power systems, IEEE Transactions on Smart Grid 13 (4) (2022) 2959–2972.

[9] S. Wang, Y. Ma, K. Sun, J. Wang, H. Li, L. M. Tolbert, F. Wang, Modeling and control of variable speed drive based loads for grid primary frequency support, IEEE Transactions on Power Delivery 38 (2) (2023) 1219–1229. doi:10.1109/TPWRD.2022.3211181.

[10] M. Malekpour, R. Azizipanah-Abarghooee, F. Teng, G. Strbac, V. Terzija, Fast frequency response from smart induction motor variable speed drives, IEEE Transactions on Power Systems 35 (2) (2020) 997–1008.

[11] Y. Son, M. Blonsky, N. Guruwacharya, V. R. Chowdhury, B. Mather, Autonomous grid support functionality in variable-speed drive-based end-use loads, IEEE Transactions on Power Electronics 39 (10) (2024) 12177–12182.

[12] Z. Mirza, H. Jain, Automated fast frequency response from inverter-based motor loads, IEEE Transactions on Smart Grid (2025) 1–1.

[13] Z. Mirza, H. Jain, Implementing grid supportive behavior in induction motor-driven loads using field oriented control, in: 2023 IEEE PES GTD International Conference and Exposition (GTD), 2023, pp. 28–32.

[14] A. T. de Almeida, P. Fonseca, P. Bertoldi, Energy-efficient motor systems in the industrial and in the services sectors in the european union: characterisation, potentials, barriers and policies, Energy 28 (7) (2003) 673–690.

[15] R. Marino, P. Tomei, C. M. Verrelli, Induction motor control design, Springer, 2010.

[16] Ieee standard for interconnection and interoperability of distributed energy resources with associated electric power systems interfaces. URL https://standards.ieee.org/ieee/1547/5915/


979-8-3315-8138-1